Understanding plasma and power characteristics of a self-generated steam bubble discharge

Maria C. Garcia,[1] Sarah N. Gucker[2] and John E. Foster[2,3]

[1] Departamento de Física Aplicada, Universidad de Córdoba, Edificio A. Einstein (C-2), Campus de Rabanales, Córdoba 14071, Spain, email: fa1gamam@uco.es

[2] Department of Nuclear Engineering and Radiological Sciences, University of Michigan, Ann Arbor, MI, 48109, USA

Abstract

Plasma formation in a self-generated steam bubble is studied using a coaxial discharge tube with axial powered electrode (nominal peak operating voltage 2000 V) and external ground lead without any gas flow. The discharge is potentially attractive for water purification applications in that the production of reactive nitrogen species and the associated water acidification is avoided. The discharge was found to form after a finite delay, which is attributed to the vapour bubble formation necessary for plasma ignition. Steam bubble composition was confirmed using emission spectra. Plasma properties and power dissipated in the self-generated steam bubble were characterized using emission spectroscopy and Lissajous methods. Discharge density and gas temperature were found to vary significantly over the applied ac voltage cycle. The power dissipated as inferred from the Lissajous method was found to scale inversely with frequency over the low frequency range investigated (4 kHz and 5 kHz).

PACS: 52.25.Os; 52.50.Dg; 52.70.Kz; 51.50.+v; 52.20.-j; 52.27.Cm; 52.40.Hf; 52.80 Wq

Keywords: low frequency plasma bubbles, atomic emission spectroscopy, atmospheric pressure.

[3]Author to whom any correspondence should be addressed

1. Introduction

Advanced water treatment methods have been the subject of significant research in recent times. Emerging threats from contaminants such as pharmaceuticals and industrial runoff has highlighted the need for advanced treatment methods [1-5]. Current water treatment technology relies primarily on filtering and disinfection and in general does not address organic chemical contaminants directly. In response, current water treatment research focuses on the removal or the safe decomposition of these contaminants. While there is significant interest in bioremediation as a safe method to addressing organic contaminants, the associated long decomposition times suggests that this approach should be supplemented or even replaced using advanced oxidation methods [6]. Advanced oxidation methods involve those processes that generate large amounts of the OH radical. The OH radical destroys organic contaminants via mineralization where the final products are typically carbon dioxide, water, and inorganic salts [4,5]. Advanced oxidation methods can be achieved conventionally. Such methods require storable precursors such as hydrogen peroxide or ozone. In recent years, the use of plasma to produce advanced oxidation products in liquid water has been the subject of many investigations. A review of research to date regarding plasmas in liquids with applications to water purification may be found elsewhere [7-9]. The interaction of plasma with liquid water introduces a host of oxidants in the water such as OH, ozone, UV light, shock waves/ultrasound, excited nitrogen species, and solvated electrons [10-18]. These reactive agents can be produced in the plasma discharge with air as the feed gas. The use of regular air eliminates the need for storables such as oxygen or hydrogen peroxide.

While the use of plasma in liquid water is certainly a promising development in the area of water purification, it is now well known that air plasmas interacting with liquid water gives rise

to acidification [19,20]. Here pH values as low as 2 are observed. Indeed, this acidity response has recently been touted as an on demand disinfectant method with applications in the plasma medicine arena. Acidification is not desirable for drinking water, however, and thus would require post processing to adjust pH. Low pH also tends to corrode water pipes. pH adjustment of treated water as a process step is not uncommon and is usually carried out at treatment plants through the addition of neutralizing agents [21].

The direct injection of advanced oxidation products into liquid water via plasma interaction is highly desirable. Plasma-based methods that do not lead to acidification would therefore greatly simplify implementation of plasma into some future water purification methodology.

Presented herein is a plasma discharge source that does not use air as the feed gas. The source self-generates vapour from the liquid media in which it is immersed. Plasma subsequently forms in this vapour bubble. The plasma source used in this implementation is an underwater dielectric barrier discharge plasma jet operated without gas flow. The steam plasma contains predominantly OH and H species. Absent are appreciable concentrations of oxygen or nitrogen-based radicals. The formation of the vapour bubble is not completely understood. It is also not clear how the vapour bubble is maintained once that the plasma has formed; that is what are the energy transfer mechanisms that maintain the bubble.

Self-generated bubble discharges have been studied in the past. Such embodiments are reviewed in Bruggeman and Leys [8] for example. Kurahashi and colleagues [22] studied self-generated bubbles in water using an rf excited electrode at reduced pressure (~150 Torr). In that work, discharge formation followed localized bubble formation at the powered electrode. Plasma formation however was intermittent with bubble collapse occurring, followed by electrolysis.

Here electrolysis was postulated as the bubble forming mechanism. Microwave generated steam bubbles with subsequent plasma formation has also been studied [23]. Schaper and colleagues [24] studied plasma formation in a steam bubble formed at a powered electrode immersed in a high conductivity saline solution. Bubble formation in this case was shown to be due to localized boiling driven by ohmic heating near the electrode. In the present work, the water is deionized and thus low conductivity. Bubble formation was observed to occur at low frequency excitation followed by the formation of a stable bubble. A plasma discharge subsequently forms in this bubble. The bubble formation mechanism in this case is less clear.

Intuitively, one would expect that the bubble is maintained by both evaporation driven by the discharge attachment at the water bubble interface and volume heating of the vapour within the bubble. In this regard, the evolution of the streamer in the vapour bubble is of interest. While some insight into the discharge mechanics can be gleaned from I-V waveform analysis, direct measurement of in volume plasma properties yield specific insight into streamer-vapour ionization processes. It is therefore of interest to understand the nature of the electron density variations over a cycle. For example, it is of interest to determine if the discharge is present on both the negative and positive portions of the cycle. Furthermore, if the plasma is present during both the negative and positive portion of the cycle, it is of general interest to know how the ionization rates vary during the cycle. One can anticipate some differences if the discharge is indeed active on both portions of the cycle as ionization mechanisms for positive and negative streamers are distinctly different. Heavy particle temperature is also of interest as it gives insight into the thermal nature of the plasma; that is, the bubble gas temperature gives insight on the nature of energy transfer to the vapour state. Does gas temperature vary appreciably over the cycle? Heavy particle temperature variations over a cycle imply time dependent reaction rates.

To address these questions, in this work we characterize the nature of the plasma discharge including the formation of the vapour bubble, the evolution of the plasma density with phase of the applied low frequency, and the evolution of the gas temperature using optical diagnostics which include emission spectroscopy and a fast frame rate camera. The power dissipated in the discharge is quantified using the Lissajous method [25,26].

2. Experimental

Plasma bubbles generation

The discharge apparatus used in this investigation is an underwater DBD plasma jet. A detailed description of the plasma source may be found elsewhere [27]. A schematic of the apparatus is shown in Figure 1.

In this work, the source operates without any input gas. Briefly, the source consists of a 6.4 mm diameter quartz or alumina dielectric tube in which a powered copper electrode (2.5 mm diameter) is centrally mounted. The grounded, return electrode consists of a molybdenum coil located near the exit plane of the source. The discharge tube, approximately 15 mm long, was fully immersed in the liquid. When voltage is applied to the submerged source, a discharge confined to a self-generated bubble located just downstream of the tube exit forms as shown in Fig. 2. The source has some similarities to the discharge apparatus investigated by Kurahashi et al in [22], though the plasma bubble produced in this work is essentially steady state and not cyclically produced as in the aforementioned case. The discharge plasma is sustained using an Elgar 501sl power supply, which could be operated at variable ac frequencies ranging from 1 kHz to 5 kHz, and a high voltage (HV) step-up transformer (50:1). Nominal peak operating

voltage was approximately 2000 V. In the present work, deionized water with a conductivity of 5 $\mu S/cm$ was used. Deionized water was used to minimize effects due to conduction ions. This way breakdown phenomena and associated plasma induced chemistry could be isolated.

The voltage relative to ground for each electrode was measured using a LeCroy2-GHzoscilloscope in conjunction with a Tektronix 20-kV high-voltage probe. The discharge current was measured using a 6595 Pearson coil. The time origin was the start of the rising of the HV pulse. A 2 nF capacitor, indicated in Fig. 3 was used for power methods via the Lissajous method.

Diagnostics

In this work, time-resolved optical emission spectroscopy (OES) techniques were employed to diagnose plasma inside the steam bubbles generated in water. Figure 3 schematically depicts the experimental setup used to acquire the OES measurements. Light emission from the plasma bubbles was analyzed by using a Czerny-Turner type spectrometer (Acton Series, SP-2300i) of 0.3 m focal length equipped with a 1800 grooves/mm holographic grating and a fast (2.5 ns gate) intensified CCD camera (PI-MAX3, Princeton Instruments) was used as a detector. Emission from the bubble, which was channeled into the spectrometer via optical fiber, was acquired at different time points during the phase of the discharge voltage. Acquisition was synchronized using a delay generator. The initializing trigger pulse is sent from the power supply which triggers both the spectrometer and the oscilloscope. The ICCD sends out a TTL pulse to the scopethat indicates the position in time in which the spectra is acquired so that one can correlate emission with waveform phase.

Figure 4 depicts discharge current and voltage signals for a typical operating point. As can be seen in the plot, the current and voltage are out of phase before breakdown. The current and voltage spike suggest breakdown. Prior two breakdown, the phase difference between current and voltage suggests capacitive reactive. Here the early current observed is likely in part displacement current coupled with low level ionic condition. A portion of the current rise before the observed breakdown is presumably associated with field and thermal processes related to bubble formation as will be discussed later. Past studies of bubble formation on electrodes in pulsed corona discharges also observe this pre-discharge curent rise [28]. An ICCD gate of 2 μs was used in this work. At each phase point, serveral accumulations (from 100 to 400) were acquired in order to increase the signal-to-noise signal ratio.

The apparatus slit function for the spectrometer was measured using 632.8 nm light produced by a He-Ne laser. The line 632.8 nm Ne I was recorded and its shape (mainly due to the instrumental broadening) fit quite well to a Gaussian profile with a FWHM of 0.14 nm.

Emission spectra acquired were corrected for the wavelength dependent sensitivity of the spectrometer and allow for the determination not only of the gas composition making up the plasma but also plasma gas temperature and electron number density over time during an voltage cycle.

3. Results

Steam Bubble formation

The formation of the steam bubble in which the plasma forms was studied using high-speed photography. A RedlakeMotionPro HS-4 camera, which was capable of recording select regions of interest at frame rates over 200,000 fps, was used in this work. Here, images are taken with the minimum exposure time of the system (1 μs). To achieve such high frame rates, the region of interest was 8 x 148 pixels, allowing for local measurements of a section near the exit plane that included the surface of the bottom of the powered electrode and a region approximately 4.5 mm long below the imaged electrode surface. It was found that the primary steam bubble in which the plasma forms is generated by microbubble formation at the surface of the electrode. Figure 5 shows images taken near the electrode surface over the voltage cycle.

The snapshots are taken over the voltage cycle as shown. What is clear is that within a microsecond of the application of power to the electrode, a change in reduced index of refraction is apparent at the electrode surface as well as the formation of a bubble at the exit plane of the quartz tube. The measurements suggest that the bubble formation, which can occur on times scales less than a microsecond. This is in contrast to other studies in which bubbles are formed directly, for example by microwaves or by dissipation in the fluid in saline solutions [27,28]. In general, this formation time had large shot to shot variability ranging from milliseconds to tenths of seconds. The fact that the water is deionized eliminates strong electrolysis effects as the source of the bubble formation. Emission spectra produced once the plasma is formed are also inconsistent with electrolysis derived bubbles. Further study of the liquid water density changes local to the electrode is required to elucidate mechanisms. Once the bubbles form, they coalesce and grow ultimately forming a nearly steady state steam bubble. The time delay associated with bubble formation was somewhat variable from start up shot to shot but on average was in the few microsecond range. Subsequent to bubble formation is breakdown that gives rise to the

generation of the discharge plasma. The spikes in the I-V characteristic are believed to be associated with this breakdown, as it was found that plasma decayed away by the time the voltage zero crossing occurs (discussed later). Figure 5b illustrates the finite delay between application of power to apparatus and the appearance of the discharge. Here light as detected by a fast photodiode, along with applied voltage (V1), voltage across the capacitor (V2, present for the Lissajous method), and discharge current is shown. The pre-discharge regime is clearly observed here appears to last for roughly one millisecond. The rapid increase in the optical signal and distortion of the current signal indicates the presence of discharge plasma.

To summarize, the plasma is initiated by first vapour formation. Here, presumably power is dissipated locally heating the water resulting in index of refraction changes in the general vicinity of the powered electrode and ultimately small bubble formation at the electrodes. The proliferation of these bubbles on the electrode surface leads to coalescing, generating ultimately the macrobubble. An associated increase in gap impedance due to the isolation of the electrode from the vapour bubble subsequently leads to breakdown once the voltage across the bubble exceeds the sparking potential. The bubble is presumably maintained after formation by localized heating of the surrounding water as the electrode itself is completely isolated from the surrounding water once the macro-sized bubble actually appears.

Emission spectra

Figure 6 shows typical optical emission produced by the steam plasma (in this case, for f = 5 kHz). As can be seen in the spectra, the most prominent peak is OH emission (3060 Å system,

band head 308.9 nm). Emission of H_α and H_β atomic hydrogen Balmer series lines is also observed.The predominance of water-related emission supports the notion that the plasma consists of mostly gaseous water vapor fragments. Copper is also observed in the spectra (Cu I 324.7 and 327.4 nm lines were particularly intense). Its presence is likely due to electrode evaporation. Na I 589.0 and 589.6 nm lines were also detected.The presence of sodium is attributed to ablation of the quartz tube though plasma interaction.

The intensity of these emissions varied over the voltage cycle, as it is more clearly shown in Fig. 7. For each intensity measurement represented in Fig. 7, three spectra were recorded. The experimental indetermination, estimated from the dispersion of the three intensities measured, never exceeded 15 %.

All emission spectra plots start at essentially t = 0 corresponding to the rise in voltage above the zero crossing point. In all cases, the species had a strong time dependence essentially rising and peaking with the absolute value of the voltage and decaying afterwards. On average the 4 and 5 kHz intensity profiles are shifted by 50 microseconds, consistent with the difference in applied voltage period. What stands out in the plots is that the discharge as inferred by the emission is more intense during the positive portion of the cycle. With the exception of OH, during the positive portion of the cycle, despite the frequency difference, most species peak in emisson at roughly the same time. The apparent phase shift in the OH spectra may also be due in part to the temporal variablity in the discharge emission associated with its unsteady motion within the steam bubble.

The higher emission intensity during the positive portion of the cycle is interesting in that the current actually has a slightly larger amplitude during the negative portion of the cycle. The similarities between the current and voltage waveforms in the face of asymmetries in intensity over the cycle suggests that electron energetics may be important. Electron temperature during the positive portion of the discharge may be higher. During the positive phase of the discharge, a positive streamer must be present and electrode processes are not expected to be important. In this regard, to maintain the ionization rate, the electron temperature would have to be higher during the positive portion of the cycle. During the negative portion of the cycle, thermionic emission is possible thus relaxing the ionization requirements for gas phase electron production. Future investigation will require measurement of the electron temperature, a quantity not well characterized in general in discharges in liquids [8]. Differences in electron energetics give rise to differences in rate constants and thus chemistry.Tailoring the duration of negative and positive portions of the voltage cycle could potentially be a means of further tailoring the reaction rates both in the bubble and at the interface.

The excitation energy threshold for the hydrogen lines is considerably higher than that of the cupper line and OH lines (the energy of the upper level corresponding to the Cu I 327 nm line and OH band head are 3.78 eV and 4.94 eV, in contrast to values over 12 eV for the hydrogen levels). In this regard, populations of cupper and OH levels are likely driven by bulk plasma population. The hydrogen lines on the other hand would be more sensitive to the electron tail and therefore may be expected to be more sensitive to polarity. Reduced electron temperature owing to thermionic emission is likely present during the negative cycle. In this regard, consistent with the spectra, H line spectral appears less intense during the negative cycle.

Gas temperature

Because nitrogen species were not present, methods based in gas temperature determination from analysis of N_2, N_2^+ spectra, could not be employed. The gas temperature (T_{gas}) was instead determined from the rotational temperature deduced from the theoretical simulation of OH(A-X) spectra and their comparisons to the experimental ones. The spectra was simulated using LIFBASE software developed by Luque and Crosley [29]. In these simulations, an instrumental resolution of 0.14 nm was used. Figure 8 illustrates a typical fit using LIFBASE.

The effective lifetime of OH (A) states in presence of water is about 0.6 ns for a temperature of 2800 K [30]. Time scale for thermalization of OH(A) rotational distribution in water is smaller than in other gases, ranging between 0.25 ns (for low-lying rotational levels) and 4 ns (all levels) [31]. Thus, because the thermalization time was similar to the effective radiative lifetime (and even larger for higher rotational levels), the values of T_{gas} measured could only be considered as an estimation of this parameter.

For the two conditions of frequency studied, gas temperature also showed variation over the cycle (see Fig. 9).

In general, gas temperatures were higher for 4 kHz case, consistent with the longer active heating over a cycle in comparison to the 5 kHz case. The data suggest that the gas tempertures tended to vary over the cycle ranging froom 2000 K to 3000 K near the peak of the cycle. The peaking of the temperature near the peak in voltage and current implies maximal deposition at this phase point. Indeed, the discharge behaves resistively as the current and voltage signals are largely in phase during the operation of the discharge. These cyclic gas temperature, like those

observed with the emisison excitation rates, suggests that reaction chemistry is also augemented by a thermal component as well.

Figure 2 depicts the typical discharge operation in this case with an alumina dielectric tube. As can be seen, the discharge emanates from the exit plane of the discharge tube in a fan like pattern, terminating at the water interface. The steam bubble itself is flattened into an elliptical shape. Thermocline-like regions are visible near the bubble as inferred from index of refraction changes in the water. The discharge and bubble size was roughly stable. The stability in size suggests that some fraction of input power must go into sustaining the vapour state of the bubble. The volume of the steam bubble shown in Fig. 2 can be estimated. The length of the major axis is roughly 0.95 cm and the minor axis can be taken to be 0.268 cm making the volume approximately 0.036 $cm^3$and a surface area of 0.65 cm^2. To produce this bubble (converting an equal volume of liquid to steam), 92 J must be input into water. The power required to maintain the bubble can be estimated using the heat flow equation:

$$H = k \cdot \frac{\Delta T \cdot A}{l}$$

where k is the thermal conductivity of liquid water, A is the contact area of the bubble, l is the characteristic size of the bubble, and ΔT is the temperature difference between the hot gas in the bubble and the ambient liquid.

The estimated power flow out of the ellipsoid shaped bubble was determined to be approximately 45 W. This estimate is based on extrapolated steam thermal conductivity.

Emission spectra suggest that steam temperature may be as high as 2800 K. The steam thermal conductivity was estimated by linear extrapolation (at 1 Atm, *k* varies linearly with temperature) [32]. It should be pointed out that at this temperature and above, thermal disassociation of steam can occur which would in turn affect the value of the thermal conductivity. The above calculation is therefore a rough estimate and in many respects a lower limit assuming that the steam remains mostly gaseous.

For self consistency, the power consumed in the discharge was also estimated using Lissajous methods.The discharge itself is essentially an underwater DBD source,which justifies the use of Lissajous methods. Figure 10 shows the resulting Lissajous figures for the 4 and 5 kHz cases.

The power was estimated by taking the product of the area of the Lissajous figure and the frequency. The large capacitance associated with the liquid water is evident in the lack of slope along the sides of the Lissajous figure. The tangent of the angle associated with the sides is equal to the reciprocal of the capacitanceassociated with the water dielectric. As can be seen here, the power consumedas determined from the Lissajous method is of similar magnitude as that estimated from the bubble size discussed earlier. The consistency of the Lissajous measurment with the order of magnitude crude energy loss calculation discussed earlier suggests that a signifiant amount of power is deposited into bubble formation and maintenance. Once the vapor bubble is actually formed, the actual power required to maintain the vapor bubble is likely much less than the crude estimate. Here the vapor bubble is most likely supported by discharge heating, thereby elimating the need for the heat of vaporization from the liquid state. At 4 kHz, the discharge consumed 72 W while at 5 kHz, the power consumption was only 56 W. It should be pointed out that consistent with intuition the power dissipated in the 4 kHz case is larger than

the 5 kHz case. In this case, the discharge acts on both the water medium and discharge for a longer duration in the lower frequency case, giving rise to a more prounced heating at the reduced frequency. This power measurement is also consistent with the measured temperatures in the gas bubbles inferred from the OH emission, which showed the gas to be consistently hotter for the 4 kHz case.

Plasma Electron Density

The discharge electron density (n_e) was inferred from the Stark broadening of H_β (486 nm) atomic hydrogen Balmer series line whose profile shape is very sensitivity to the micro-field induced by charged particles (electrons and ions) that surrounds the emitter atom (H) [33,34]. This line is commonly employed for determination of electron densities as small as 10^{20} m^{-3}.The Stark full width at half maximum (FWHM) of this emission line has a very weak dependence on the plasma electron temperature, on the emitter–perturber reduced mass and on kinetic equilibrium conditions in the plasma, making the use of line especially convenient for discharges in liquids [35,36]. The Stark FWHMs have been theoretically calculated and tabulated by Gigosos *et al.* for wide ranges of electron densities [36].

It was assumed that the profile of the emitted H_β line as a Voigt profile, a convolution of a Gaussian shape profile and a Lorentzian shape profile, Gaussian contribution is attributed to the *Doppler and instrumental* broadening of the line, and Lorentzian part is associated with *van der Waals* and *Stark* broadenings [34-35].

From the best Voigt profile fit, the actual *Stark* width ($\Delta\lambda_{Stark}$) of the H_β line was determined. It should be pointed out that the contributions of *Doppler* broadening ($\Delta\lambda_{Doppler}$) and

van der Waals broadening ($\Delta\lambda_{vdw}$) to the FWHM were calculated using expressions given by Bruggeman *et al.* in ref [35]:

$$\Delta\lambda_{vdw} = \frac{4.10}{T_{gas}^{0.7}}(nm)$$

$$\Delta\lambda_{Doppler} = 3.48\times10^{-4}T_{gas}^{1/2}(nm)$$

Finally, using Gigosos et al. [36] tables, the electron density was calculated. The electron density can also be found directly using the following equation [35]

$$\Delta\lambda_{Stark} = 4.8\ nm\times\left(\frac{n_e}{10^{23}m^{-3}}\right)^{0.68116}$$

Figure 11 shows the values of electron density over a cycle for both 4 kHz and 5 kHz cases, measured from the Stark width of H_β line.

Although the H_α line is more intense than H_β line, it is almost never used to measure electron densities especially for small electron densities due to several reasons. First of all, because of the smaller value of its Stark FWHM, sometimes close to the spectral resolution. Also, due to the strong effect on its width of the ion dynamics [35], i.e. the strong dependence of H_α line FWHM on the emitter–perturber reduced mass and on kinetic equilibrium conditions in the plasma; this forces to know both composition of the plasma (perturbers of H) and electron temparature and gas temperature ratio, when using this line for n_e determination. Finally, this line may suffer strong self-absorption [37], effect difficult to quantify in plasmas in water.

As can be seen in both cases, the electron density peaks during the positive portion of the cycle. The magnituide of the densities are similar independent of frequency. This is likely attributed to the notion that the discharge formed is due to an overvoltage; that is, once at breakdown is achieved, additional power is not transferred to the arc-like short. Additionally, the period of the cycle whether 4 or 5 kHz is long compared to the plasma decay time. The peaking of the discharge density during the positive portion of the cycle is consistent with these measured plasma density changes. The data appears to suggest that the source is most efficienty at producing plasma during the positive portion (positive streamer) of the discharge. When the electrode is positive, electrode processes such as melting and thermionic emisison—both of which are energy losses—are not important. Finally, it should be pointed out that the disparity in electron density over the negative portion of the cycle is consistent with the observed trends in plasma-induced emission and gas temperature.

4. Concluding remarks

The steam based plasma discharge offers the prospect of eliminating the acidification problem observed in air plasmas in contact with liquid water. In this work, the time evolution of this discharge type was elucidated using high speed photography, emission spectroscopy and Lissajous methods. It was found that bubble formation was fast, ~ microseconds. The plasma changes character over an the voltage cycle not unlike that which is observed when the source is operated on air [38]. Plasma density was found to follow the emission as inferred from Stark broadening measurements. Gas temperature for this discharge was found to range to 2000 K to nearly 3000 K, which places the discharge in the quasi-nonequilibrium category as this

temprature is expected to be much less than the electron temperature (10 x lower). The gas temperature and plasma density vary over time, which suggests that one can expect chemical reactivity also varies over time with the average reactivity manifesting itself as a weighted time average. Interestingly, temperature was found to be lowest during the negative portion of the cycle. Dissipated power measurements suggest that power consumed is dominated by steam bubble formation and maintenance. Future work will involve understanding the scaling of the discharge perhaps using multiple applicators in parallel. If localized heating is critical to bubble formation then local water flow past the applicator, as would be expected in any inline system, will be important as it would lead to convective cooling effects which should affect the energy balance for steam bubble maintanence. Currently, based on the results of this study, discharge power consumption is somewhat high. This energy consumption rate may preclude the application of this source for large scale applications. It may however be applicable for specialized point of use applications such as reuse applications such as water resuse supporting human spaceflight. In this case, the competing technology is currently low pressure distillation which is energy intensive [39].

Acknowledgments

This work was supported in part by the National Science Foundation under Grant CBET 1033141 and Grant CBET 1336375, and in part by the National Science Foundation Graduate Student Research Fellowship under Grant DGE 0718128.

References

[1] Andreozzi R, Caprio V, Insola A and Marotta R 1999 Catalysis Today **51** 53.

[2] Klavarioti M, Mantzavinos D and Kassinos D 2009 Environment International **35** 402.

[3] Carey JH 1992 Water Poll. Res. J. Canada **27** 1.

[4] Munter R 2001 Proc. Estonian Acad. Sci. Chem. **50** 59.

[5] Glaze WH, Kang JW and Chapin DH 1987 Ozone: Sci. Eng. **9** 335.

[6] Oller I, Malato S and Sanchez-Perez JA Science of the Total Environment 2011 **409** 4141.

[7] Locke BR, Sato M, Sunka P, Hoffmann MR and Chang JS 2006 Ind. Eng. Chem. Res. **45** 882.

[8] Bruggeman P and Leys C 2009 J. Phys. D: Appl. Phys. **42** 053001.

[9] Foster J, Sommers BS and Gucker SN 2012 IEEE Trans. Plasma. Sci. **40** 1311.

[10] Sahni M and Locke BR, Ind. Eng. Chem. Res. 45, 5819, 2006

[11] Clements JS, Sato M, and Davis RH, IEEE Trans. Ind. Appl., IA-23, 224, 1987

[12] Sun B, Sato M, Clements JS, J. Phys. D: Appl. Phys., 32, 1908, 1999.

[13] Nemcova L, Nikiforov A, Leys C, and Krcma F, IEEE Trans. Plasma Science, 39, 865, 2011.

[14] Kirkpatrick MJ, and Locke BR, Ind. Eng. Chem. Res., 44, 4243, 2005

[15] Yamabe C, et al, Plasma Process. Polym., 2, 246, 2005.

[16] Sahni M, Finney WC, and Locke BR, 2005, J. Adv. Oxid. Technol., 8, 105,.

[17]Tezcanli-Guyer G. and Ince, 2004, NH, Ultrasonics, 42, 603.

[18] Sano N et al 2002 Ind. Eng. Chem. Res., 41, 5906.

[19] Graves DB 2012 J. hys. D: Appl. Phys. **45** 263001.

[20] Oehmigen K, Hähnel M, Brandenburg R, Wilke C, Weltmann KD and von Woedtke T, Plasma Process. Polym. 2010 **7** 250.

[21] Faust SD and Aly OM 1998 Chemistry of Water Treatment, 2nd ed., Ann Arbor Press, Chelsa.

[22] Kurahashi M, Katsura s and Mizuno A 1997 J. Electrostatics **42** 93.

[23] Nomura S, Toyota H, Mukasa S, Takahashi Y, Maehara T, Kawashima A and Yamashita H 2008 Applied Physics Express **1** 046002.

[24] Schaper L, Graham WG and Stalder KR 2011 Plasma Sources Sci. Technol **20** 034003.

[25] Falkenstein Z and Coogan JJ 1997 J. Phys. D: Appl. Phys. **30** 817.

[26] Manley TC 1943 J. Electrochem. Soc. **84** 83.

[27] Foster JE, Weatherford B, Gillman E and Yee B 2010 Plasma Sources Sci. Technol. **19** 025001.

[28] Lisitsyn I, Nomiyama H, Katsuki S and Akiyama H 1999 IEEE Trans. Dielectrics and Electrical Insulation **6** 351.

[29] Luque J and Crosley DR 1999 "LIFBASE: Database and spectral simulation (version 1.5)" SRI International Report MP 99-009.

[30] Bruggeman PJ, Sadeghi N, Schram DC and Linss V 2014 Plasma Sources Sci. Technol. **23** 023001.

[31] Kliner DAV and Farrow RL 1999 Journal of Chemical Physics **110** 412.

[32] Beaton CF1986 Heat Exchanger Design Handbook, Chapter 5.5.3.

[33] Griem HR 1974 Spectral Line Broadening by Plasmas, Academia Press, New York.

[34] Yubero C, Calzada MD and Garcia MC 2005 J. Phys. Soc. Japan **74** 2249.

[35] Bruggeman P, Schram DC, Gonzalez MA, Rego R, Kong MG and Leys C 2009 Plasma Sources Sci. Technol. **18** 025017.

[36] Gigosos MA, Gonzalez MA and Cardeñoso V 2003, Spectrochim. Acta B **58** 1489.

[37] Konjevic N, Ivkovic M, Sakan N 2012, Spectrochim. Acta B **76** 16.

[38] Foster JE, Sommers B, Weatherford B, Yee B and Gupta M 2001 Plasma Sources Sci. Technol. **20** 034018.

[39] Schmidt, R., "Water Recovery By Vapor Compression Distillation," SAE Technical Paper 891444, 1989, doi:10.4271/891444.

FIGURE CAPTIONS

Figure 1. Schematic of underwater DBD plasma jet. For these experiments, no gas was injected.

Figure 2. Photograph of discharge in self-formed steam bubble. Also visible are gradients in the index of refraction, which is indicative of heat transfer between bubble and surrounding medium

Figure 3. Schematic depiction of apparatus.

Figure 4. Typical voltage and current variation in time (4 kHz example).

Figure 5a. Early stages of bubble formation (before plasma formation).Frames taken over a voltage cycle; (a), taken at -5 μs from the start of the voltage cycle; (b), 0 μs; (c), 50 μs; (d), 100 μs; (e), 150 μs; (f), 195 μs; (g), 200 μs.

Figure 5b. Time evolution of discharge voltage and current with time with following initial application of voltage.

Figure 6. Typical steam plasma emission spectra.

Figure 7. Time variation in OH, Cu, and H emission over a cycle with AC frequency.

Figure 8. Simulated spectra fit to observed OH emission.

Figure 9. Gas temperature variation over a cycle inferred from OH emission.

Figure 10. Lissajous figures for the steam discharge.

Figure 11. Electron density over the cycle measured from H_β Stark broadening.

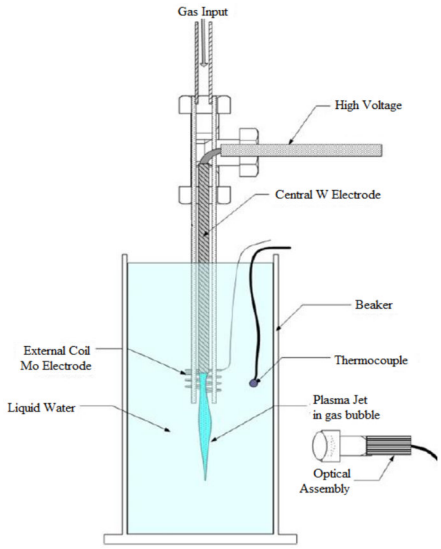

Figure 1. García et al.

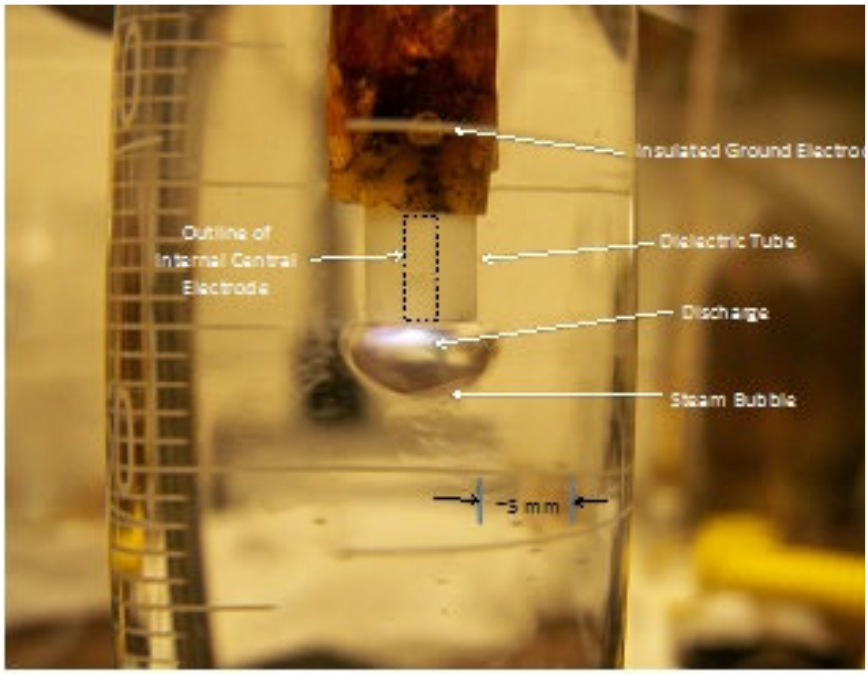

Figure 2. García el al.

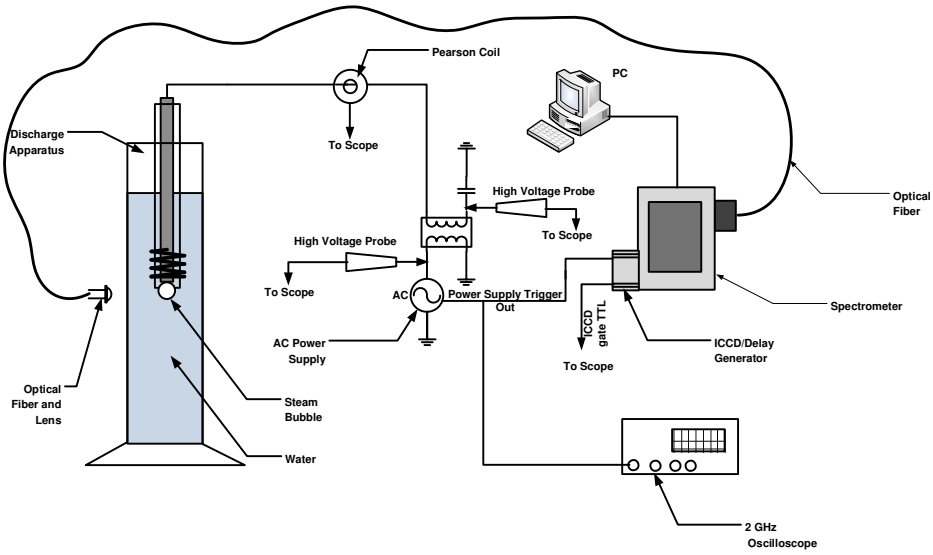

Figure 3. García et al.

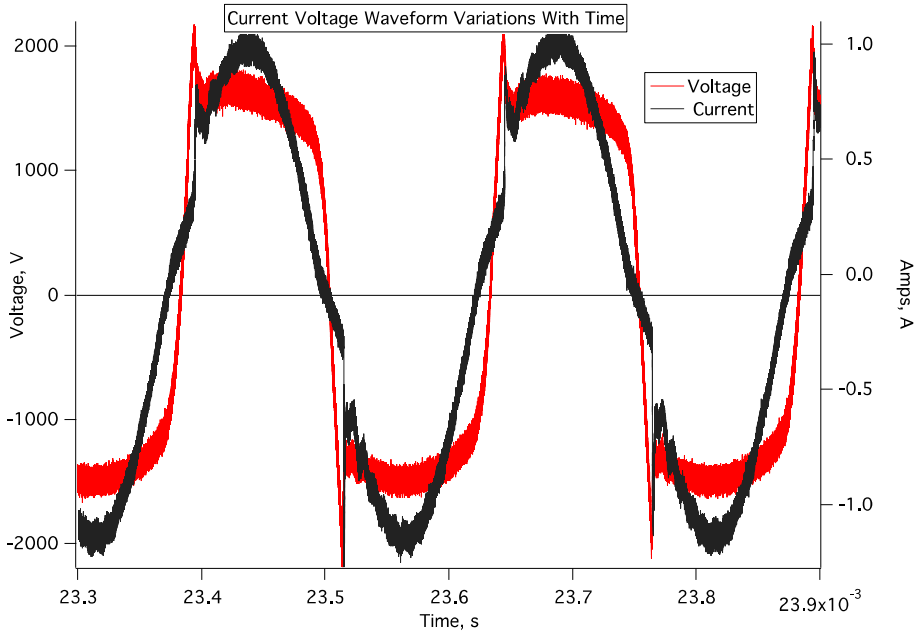

Figure 4. García et al.

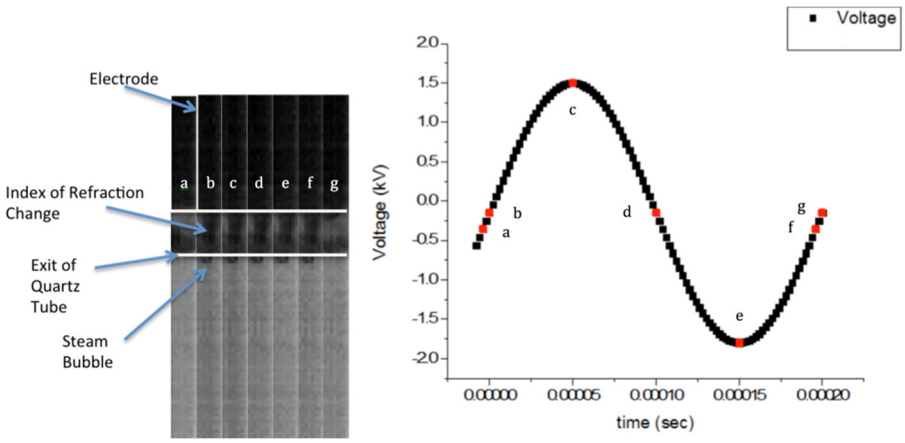

Figure 5a. García et al.

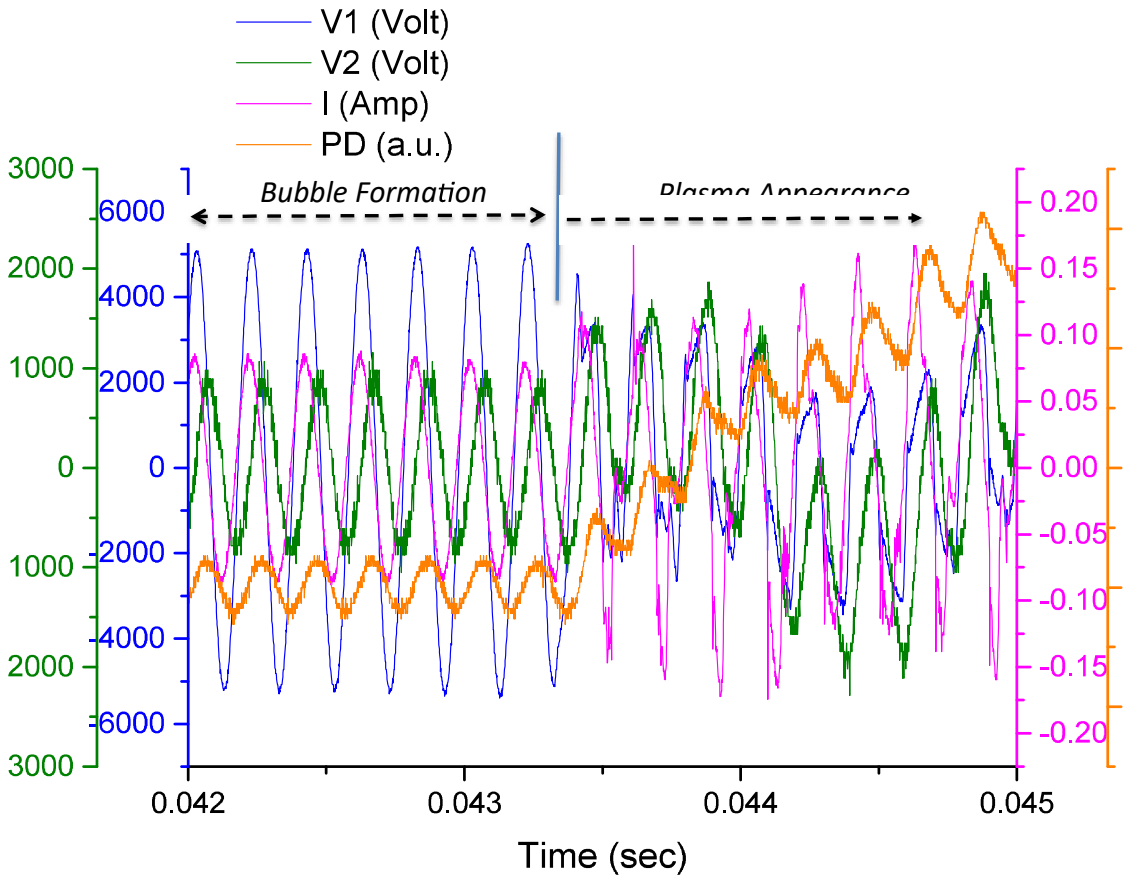

Figure 5b. García et al.

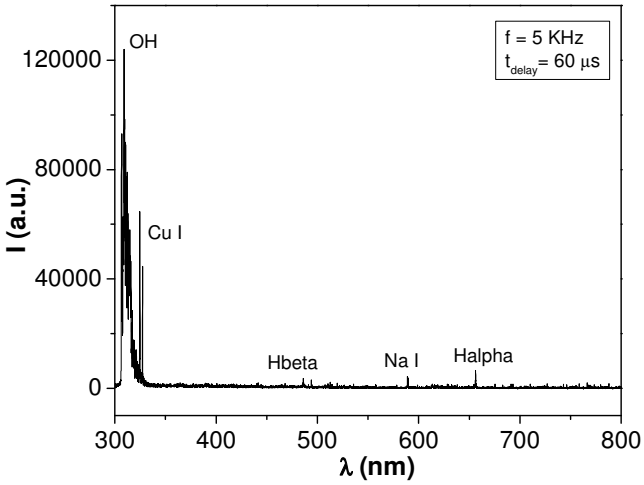

Figure 6. García et al.

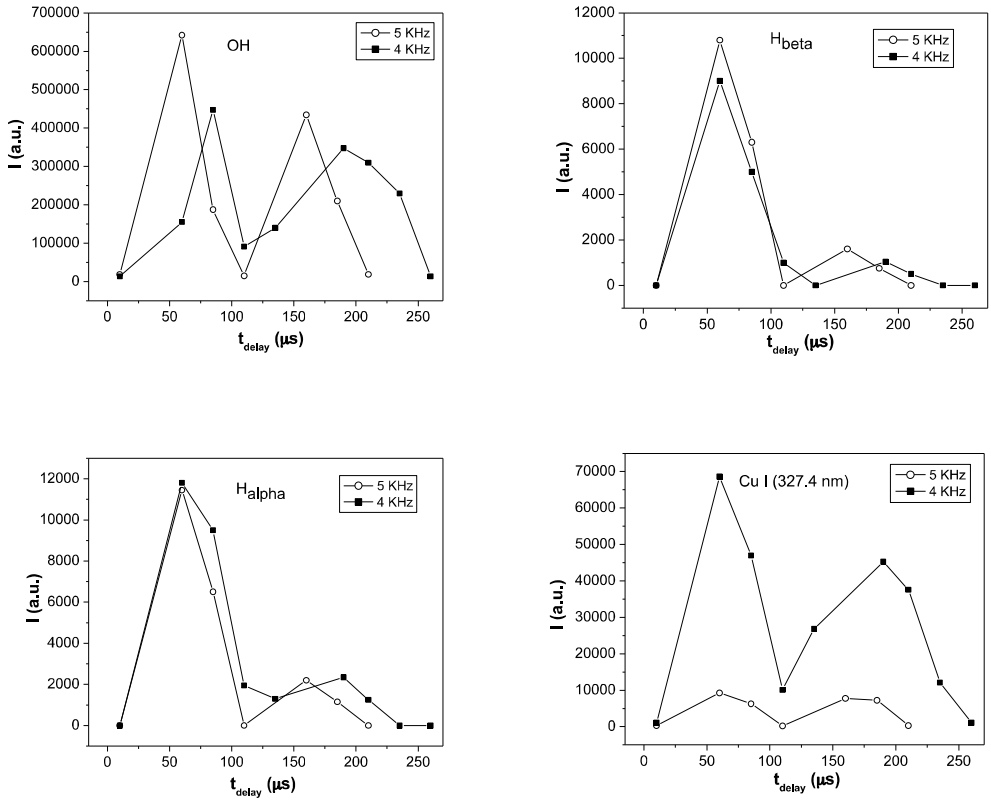

Figure 7. García et al.

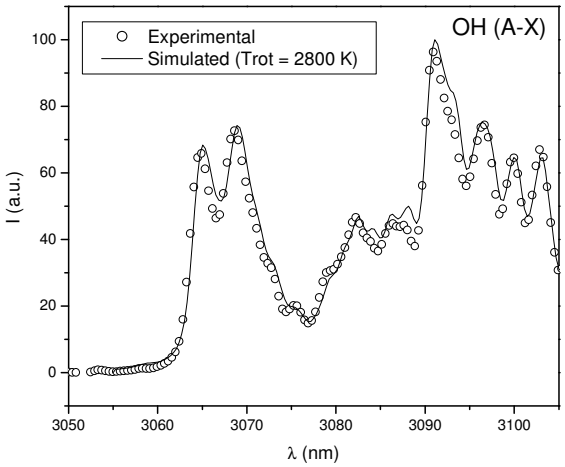

Figure 8. García et al.

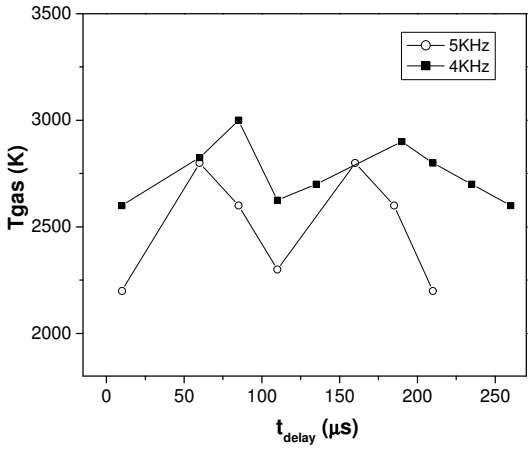

Figure 9. García et al.

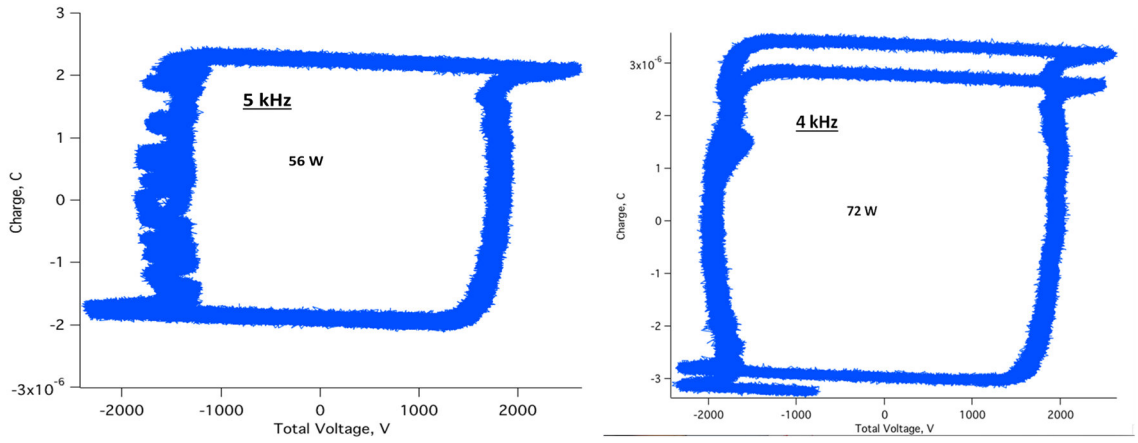

Figure 10. García et al.

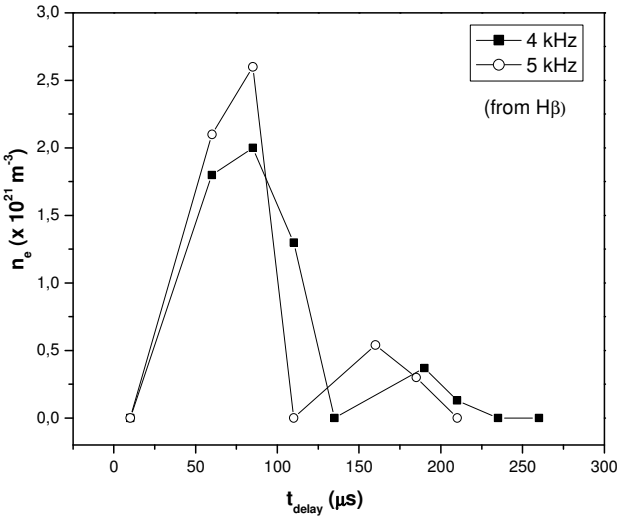

Figure 11. García el al.